

Published in final edited form as:

NanoImpact. 2022 April; 26: 100401. doi:10.1016/j.impact.2022.100401.

Differential modulation of endothelial cytoplasmic protrusions after exposure to graphene-family nanomaterials

Herdeline Ann M. Ardoña^{a,1}, John F. Zimmerman^a, Kevin Shani^a, Su-Hwan Kim^{a,2}, Feyisayo Eweje^a, Dimitrios Bitounis^b, Dorsa Parviz^c, Evan Casalino^a, Michael Strano^c, Philip Demokritou^{b,3}, Kevin Kit Parker^{a,*}

^aDisease Biophysics Group, John A. Paulson School of Engineering and Applied Sciences, Harvard University, Boston, MA 02134, USA

^bCenter for Nanotechnology and Nanotoxicology, Department of Environmental Health, T. H. Chan School of Public Health, Harvard University Boston, MA 02115, USA

Department of Chemical Engineering, Massachusetts Institute of Technology, 77 Massachusetts Avenue 66-570b, Cambridge, MA 02139, USA

Abstract

Engineered nanomaterials offer the benefit of having systematically tunable physicochemical characteristics (e. g., size, dimensionality, and surface chemistry) that highly dictate the biological activity of a material. Among the most promising engineered nanomaterials to date are graphenefamily nanomaterials (GFNs), which are 2-D nanomaterials (2DNMs) with unique electrical and mechanical properties. Beyond engineering new nanomaterial properties, employing safetyby-design through considering the consequences of cell-material interactions is essential for exploring their applicability in the biomedical realm. In this study, we asked the effect of GFNs on the endothelial barrier function and cellular architecture of vascular endothelial cells. Using micropatterned cell pairs as a reductionist in vitro model of the endothelium, the progression of cytoskeletal reorganization as a function of GFN surface chemistry and time was quantitatively

CRediT authorship contribution statement

Herdeline Ann M. Ardoña: Conceptualization, Methodology, Validation, Formal analysis, Investigation, Writing - original draft, Visualization, Supervision, Project administration. John F. Zimmerman: Software, Investigation, Validation, Formal analysis, Writing – review & editing. Kevin Shani: Investigation, Writing – review & editing. Su-Hwan Kim: Software, Validation, Formal analysis, Writing - review & editing. Feyisayo Eweje: Investigation, Writing - review & editing. Dimitrios Bitounis: Investigation, Resources, Writing - review & editing. Dorsa Parviz: Investigation, Resources, Writing - review & editing. Evan Casalino: Validation, Writing - review & editing, Michael Strano: Resources, Writing - review & editing, Supervision. Philip Demokritou: Resources, Writing - review & editing, Supervision. Kevin Kit Parker: Conceptualization, Writing - original draft, Supervision, Project administration, Funding acquisition.

Declaration of Competing Interest

The authors declare no conflict of interest regarding the publication of this article.

Appendix A. Supplementary data

Supplementary information to this article containing a more comprehensive description of experimental methods, quantification protocols, and other supporting figures can be found online at: https://doi.org/10.1016/j.impact.2022.100401.

^{*}Corresponding author at: 150 Western Ave., Science & Engineering Center, Boston, MA 02134, USA. kkparker@seas.harvard.edu (K.K. Parker).

Current Address: Department of Chemical and Biomolecular Engineering, Samueli School of Engineering, University of California,

Irvine, CA 92697, USA. ² Current Address: Department of Chemical Engineering, Dong-A University, Busan, South Korea.

³ Current Address: Environmental Occupational Health Sciences Institute (EOHSI), School of Public Health, Rutgers Biomedical Health Sciences, Rutgers University, 170 Frelinghuysen Rd, Piscataway, NJ 08854, USA.

monitored. Here, we show that the surface oxidation of GFNs (graphene, reduced graphene oxide, partially reduced graphene oxide, and graphene oxide) differentially affect the endothelial barrier at multiple scales; from the biochemical pathways that influence the development of cellular protrusions to endothelial barrier integrity. More oxidized GFNs induce higher endothelial permeability and the increased formation of cytoplasmic protrusions such as filopodia. We found that these changes in cytoskeletal organization, along with barrier function, can be potentiated by the effect of GFNs on the Rho/Rho-associated kinase (ROCK) pathway. Specifically, GFNs with higher surface oxidation elicit stronger ROCK2 inhibitory behavior as compared to pristine graphene sheets. Overall, findings from these studies offer a new perspective towards systematically controlling the surface-dependent effects of GFNs on cytoskeletal organization *via* ROCK2 inhibition, providing insight for implementing safety-by-design principles in GFN manufacturing towards their targeted biomedical applications.

Keywords

2-D nanomaterials; Cytoplasmic protrusions; Nanosafety; Endothelial cells; Cell-material interactions

1. Introduction

Graphene family nanomaterials (GFNs) have emerged as an important class of engineered nanomaterials for biomedical applications due to their unique properties, such as their electrical property, mechanical strength, and high surface area (Parviz et al., 2020; Reina et al., 2017). To fully maximize the translational potential of GFNs towards biological applications, it is necessary to understand how these 2-D nanomaterials (2DNMs) interact at different biological scales for various cell or tissue types (Chng and Pumera, 2015; Fadeel et al., 2018; Murphy et al., 2015; Sanchez et al., 2012; Seabra et al., 2014). Previous reports shed light on how nanomaterials may perturb complex cellular machinery, such as by imparting genotoxicity (Watson et al., 2014) and by influencing the ability of cells to repair their DNA (Toprani et al., 2021). It is therefore important to consider the processes that occur at the cell-material interface that may dictate higher-order therapeutic or toxic effects of nanomaterials on organ systems, as well as to identify design and conditions by which they are safely deployed.

Some of the currently known mechanisms of GFN-induced toxicity include physical disintegration of cells or stress response to reactive oxygen species (ROS) production (Ou et al., 2016). There are also different proposed routes for the cellular uptake of GFNs (Alnasser et al., 2019; Kucki et al., 2017; Li et al., 2021; Zou et al., 2017), such as through non-covalently-mediated, spontaneous interaction with the cell membrane *via* its edge asperities and corner sites (Li et al., 2013; Wu et al., 2015) or *via* endocytosis (Huang et al., 2012; Wu et al., 2013). Regardless of the mechanism of interaction, similar to other nanomaterials, the biological effects of GFNs depend on dose, administration routes, and their physicochemical properties (Fadeel et al., 2018). In previous reports, variation in GFN oxidation states (*i.e.*, C/O ratio) have been shown to differentially induce cellular behavior (Contreras-Torres et al., 2017; Frontiñán-Rubio et al., 2018; Liao et al., 2011; Matesanz

et al., 2013; Pelin et al., 2017). The differential effects of GFNs with varying oxidation have also been demonstrated for *in vivo* processes such as monocyte recruitment, neutrophil influx post-intratracheal administration, or ROS production in pulmonary tissues (Bengtson et al., 2017; Li et al., 2018; Sydlik et al., 2015). Under physiological conditions, the impact of C/O ratio or surface oxidation in GFNs have also been reported to be a significant factor that affects the extent of corona formation, therefore impacting biodistribution (Bhattacharya et al., 2016). Beyond the reported effects of GFN surface oxidation on different cell types, for applications requiring transport across the vascular barrier, it is important to understand how surface properties of xenobiotic nanomaterials affect the vasculature.

Here, we ask how GFNs can potentiate functional changes on endothelial barriers via cytoskeletal remodeling, specifically the formation of extensive actin-based membrane protrusions such as filopodia and lamellipodia (Hobbs et al., 2014; Lamalice et al., 2007). Actin regulators control cell protrusion architecture, forming either branched or unbranched actin networks for lamellipodia or filopodia, respectively. Both protrusion types are important for cell morphogenesis, wound healing, metastasis, and for angiogenesis (Tsygankov et al., 2014). During angiogenesis, endothelial tip cells form cytoskeletal actin protrusions, including filopodia, needed to successfully form endothelial tissues or fill open gaps (Figueiredo et al., 2021; Lamalice et al., 2007; Rottner and Schaks, 2019). In addition, the barrier function of vascular endothelia is largely regulated by actin organization and contractility (Belvitch et al., 2018; Claesson-Welsh et al., 2021). Rho-family GTPases (RhoA, Rac1, Cdc42) are known to influence the organization, polymerization, and contractility of actin (Hobbs et al., 2014; Yao et al., 2010). RhoA/Rho-associated protein kinase (ROCK) signaling promotes migration by regulating integrin activity and membrane protrusions to the leading edge (Worthylake and Burridge, 2003). In a previous work (Eweje et al., 2019), it has been demonstrated that exposure of endothelial cells to 0-D (metal and metal oxide nanoparticles) and 1-D nanomaterials (cellulose nanocrystals) lead to formation of stress fibers and destabilization of cortical actin. These were quantified by utilizing micropatterned cell pairs as a reductionist model of barrier tissues that enables a high throughput normalization of cell morphology for nanotoxicology and drug screening applications (Eweje et al., 2019; O'Connor et al., 2020). These downstream effects of material exposure to endothelial cell architecture and tissue function are less understood for 2DNMs such as GFNs.

In this work, we hypothesize that the physicochemical properties of GFNs, specifically surface oxidation state, can differentially affect endothelial tissue function and the Rho/ROCK-mediated cytoskeletal organization of endothelial cells. We focus herein on evaluating the oxidation-dependent impacts of GFN exposure on quantifiable structural and functional parameters rather than on the mechanism of cell-material interaction. To do so, the micropatterned cell pair model was used to systematically quantify the dose-and time-dependent effects of GFNs on endothelial permeability and cytoskeletal architecture. Significant formation of cytoplasmic protrusions, lamellipodia and filopodia, were observed when micropatterned endothelial cell pairs were exposed to GFNs. These findings suggest that GFNs can have an effect on Rho/ROCK signaling, which was investigated here *via* activation assays to understand the molecular pathways or specific molecular effectors perturbed by the GFN nanomaterial exposure.

2. Results and discussion

We ask what the effects are of surface oxidation of GFNs on endothelial vascular barrier structure and function by taking a top-down approach, starting from the influence on barrier function to the effect of GFNs on molecular effectors of cytoskeletal organization. The test GFNs used here span from graphene as the reference, to graphene oxide as the most oxidized form (Fig. 1a). Graphene with 110×110 nm dimensions was used as a reference to compare the results of the three other GFNs with varying surface oxidation state and same size (400×400 nm) (Bazina et al., 2021; Bitounis et al., 2020; Duan et al., 2020; Parviz and Strano, 2018). In particular, the four GFNs evaluated in this study are as follows (Table S1): graphene in Na cholate, reduced graphene oxide (RGO) in Na cholate, partially reduced graphene oxide (PRGO) in Na cholate, and graphene oxide (GO).

2.1. GFN exposure affects endothelial barrier permeability

To assess the functional effect of direct GFN exposure to endothelial layers, we measured the permeability of two small molecular dyes (Alexa Fluor 555 and Oregon Green 488) across confluent human umbilical vein endothelial cell (HUVEC) monolayers on a Transwell as a measure of barrier integrity (Fig. 1b-c) (Bischoff et al., 2016). These monolayers were treated with GFN concentrations ranging from 0 to 50 µg/mL, which were selected based on the common range used for previous literature reports (Ou et al., 2016). Because cAMP analogs are known to promote cortical actin structures and to stabilize intercellular junctions, 8-CPT-cAMP was added to the HUVEC monolayers used for permeability measurements 24 h prior to addition of any test agents (GFNs and controls) (Bogatcheva and Verin, 2008; Breslin et al., 2015; Spindler et al., 2010). After 24 h exposure of the cAMP-treated endothelial tissue monolayers to GFNs, dose-dependent increase in permeability was observed for the more oxidized 400 nm GFNs but not for the graphene reference (Fig. 1d-g). Starting at 10 µg/mL, PRGO- and GO-treated monolayers showed a statistically significant increase in barrier permeability with respect to controls; while the RGO-treated monolayers began showing a similar trend at 25 μg/mL. This result indicated that the more oxidized GFNs (PRGO and GO) induced a perturbation on HUVEC monolayer integrity at lower doses than RGO.

At this point, it is important to note that the observed effects are compared in terms of administered dose expressed in µg/mL and duration of exposure. Ideally, the *in vitro* biological activity of GFNs would be compared based on the GFN mass delivered to cells. Such normalizations are feasible with dense and small aspect ratio nanoparticles (*e.g.*, metal oxides), for which experimental and computational dosimetry methods have been developed and embraced by the scientific community (DeLoid et al., 2017; Thomas et al., 2018). However, the non-spherical, soft, carbon-based nature of GFN precludes the use of these protocols. While experimental and theoretical studies on the particokinetics of anisotropic ENMs in liquid media are becoming available (Bitounis et al., 2019; Holt et al., 2021), there is yet to be an all-encompassing and easy-to-use method. With this, the similar lateral size, planar geometry, and chemical composition of GFNs employed in this study should translate to similar kinetics in cell culture medium and thus allowing for an approximate comparison.

To determine if the measured change in barrier function was related to cell viability, we examined the dose-dependent change in mitochondrial reductase activity through a colorimetric assay based on a tetrazolium dye (3-(4,5-dimethylthiazol-2yl)-5-(3-carboxymethoxyphenyl)-2-(4-sulfophenyl)-2*H*-tetrazolium; MTS) (Fig. S1). A dose-dependent decrease in cell viability after 24 h was observed, which was consistent with the trend in measured barrier permeability (Fig. S1a). In some conditions, the measured absorbance was higher than the control. This is indicative of an increase in mitochondrial reductase activity, therefore mitochondrial activity, similar to previously reported observations for other engineered nanomaterials (Eweje et al., 2019; Zimmerman et al., 2016). Moreover, increasing permeability indices, correlated to loss in barrier integrity, were observed for monolayers treated with GFNs with higher surface oxidation increases. These results are consistent with the association between cell death and cellular morphology contraction, and consequentially, increase barrier permeability. In cases where the viability does not significantly decrease but a significant increase in monolayer permeability is observed (i.e., PRGO at 10–50 μg/mL), other than cytoskeletal contraction, we can attribute this to the impact of GFNs on the stability of junction proteins and formation of intercellular gaps. The MTS-based viability assay also showed a significant decrease in cell viability after a 24 h exposure of HUVECs to 50 µg/mL RGO and GO (Fig. S1b). We therefore limited the GFN concentrations used throughout this work to 50 µg/mL or lower. Taken together, dose-dependent changes in barrier permeability and cell viability were observed after a 24-h exposure of HUVECs to more oxidized GFNs (RGO, PRGO, GO) at concentrations below or equal to 50 µg/mL.

2.2. GFN-triggered cytoplasmic projections of endothelial cell pairs

Cytoskeletal reorganization due to actin stress fiber formation has been established to influence focal adhesion complex structure, cell migration, and mediate retraction of cell-cell borders into endothelial gaps (Belvitch et al., 2018; Bisaria et al., 2020; Dudek and Garcia, 2001; Yao et al., 2010). Based on the measured increase in permeability upon exposure to higher concentrations and more oxidized forms of GFNs, we further explored how GFNs affect endothelial architecture at the cellular level. Micropatterned cell pairs, considered as the smallest functional repeating unit of a continuous barrier tissue representing one cell-cell junction, was utilized here as an *in vitro* model to study cellular morphology and cytoskeletal organization (Fig. 2a–b; Fig. S2). By normalizing the geometry of the cells, we can quantitatively compare cellular architecture parameters of unexposed and GFN-exposed cell pairs. A bihexagonal morphology was utilized for the cell pairs as this polygonal geometry mimics the cobblestone-like morphology of endothelial cells under physiological environments. Following a previously published protocol (Eweje et al., 2019), the endothelial basement membrane extracellular matrix (ECM) protein fibronectin was micropatterned *via* soft lithography techniques and used to generate bihexagonal cell pairs.

After a 24-h exposure to 50 μ g/mL GFNs, from the images of cell pairs with phalloidinstained F-actin, we observed significant cytoplasmic protrusions (Fig. 2c; Fig. S3–S6) that were not exhibited by HUVEC pairs exposed to 0-D or 1-D ENMs under similar culture conditions (Eweje et al., 2019). The unexposed control (no GFN) showed cortical actin, while the control with dispersant (0.45 mg/mL Na cholate) showed destabilized cortical

actin and formation of stress fibers. However, the cytoplasmic protrusions caused by the Na cholate control were not as extensive as those observed after 24 h of exposure to GFNs. These results suggest that GFNs potentially induce structural remodeling in cells that comprise vascular barriers. Under physiological conditions, cytoskeletal remodeling events, particularly lamellipodia and filopodia formation, are controlled by the Rho/ROCK signaling pathways (Hobbs et al., 2014). The key players in this pathway are RhoA (activated during stress fiber formation), Rac1 (activated during lamellipodia formation), Cdc42 (activated during filopodia formation) and ROCK (more downstream effector of actin organization) (Hobbs et al., 2014; Lamalice et al., 2007). To further explore how GFNs affect the role of these key players in cytoskeletal remodeling, cell pairs were then treated with a panel of drugs that result in Rho activation, Rho/Rac1/Cdc42 activation, Rac1/Cdc42 activation, and ROCK inhibition (Y-27632).

The resulting cell pair morphologies after these drug treatments served as references to better understand whether the mechanism by which GFNs triggers the extensive cell protrusions is *via* influencing the activity of Rho family GTPases. In a previous report, micropatterned single cells of fibroblasts showed Cdc42 activation in the vertices of the cell polygon, resulting in filopodia formation not observed in cells without any vertices (*i.e.*, those with circular morphology) (Parker et al., 2002). Despite the bihexagonal morphology of the cell pairs, the cytoplasmic protrusions of the GFN-exposed, Rho/Rac/Cdc42-activated, and ROCK-inhibited cell pairs were observed stochastically along the cell edges and without any preference to the vertices of the polygon pattern. These results further illustrate that the cell-cell interactions recapitulated by the pair model provides a distinct perspective from single cell assays that do not capture intercellular processes.

To dissect the morphological evolution of cell pairs across the time dimension, GFNexposed cell pairs were imaged at different time points (Fig. 3). The extensive cell protrusions were observed starting at 2 h across all 4 GFNs. These protrusions present structures reminiscent of lamellipodia and filopodia. We then used a previously reported tree-graph transformation-based cell mapping approach called CellGeo (Tsygankov et al., 2014) to distinguish and quantify filopodia across the cell pair samples under different exposure conditions (see SI for more details). Quantification of the filopodia protrusion parameters (Fig. 4a-b) show that GFN-exposed cell pairs have higher number of protrusions than the controls (no GFN and with Na cholate). This quantification also showed that the cytoplasmic protrusions started saturating between 4 and 8 h. Protrusion index, defined here as the ratio of number of protrusions and mean protrusion length, accounts for both the density and length of protrusions per pair and was reported for different exposure timepoints. The Na cholate-dispersed GFNs protrusion indices (Fig. 4c) are relatively higher than the other exposure conditions, whereby the most oxidized among this surfactant-dispersed subset (PRGO) have the largest protrusion index values, especially at later timepoints. By exploring the dose-dependent effects of GFNs on the formation of cytoplasmic protrusions, we observed a general increase in the number of protrusions as the dose increases from 5 to 50 µg/mL. Altogether, these combined results from cytoplasmic protrusion quantification suggests that the surface chemistry of the GFNs studied here influence the extent of cytoskeletal organization of the endothelial cell pairs (Fig. S7–9).

2.3. Influence of GFNs to the molecular effectors of cytoskeletal organization

We then asked the question, how does GFN exposure affect the expression of molecular effectors, such as small GTPases, involved in cytoskeletal reorganization? In particular, we set out to evaluate the effect of GFN-exposure on Rac and Cdc42 activation since these two small GTPases are highly correlated with lamellipodia and filopodia formation, respectively (Hobbs et al., 2014). We employed G-LISA activation assays to understand whether Rac and Cdc42 activation correlates with the extensive protrusion formation due to GFN (Fig. 5a-b). Interestingly, only the Na cholate control and graphene after 24 h showed a significantly higher Rac activation as compared with the no GFN control (i.e., untreated samples). These results suggest that there is some baseline Rac activation occurring due to Na cholate surfactant. No significant differences in Rac activation were observed between the no GFN condition against the other exposure conditions at 6 h, which is a timepoint within the window where the onset of maximum protrusion formation occurs across the different GFN exposure conditions. On the other hand, the cell pairs treated with ROCK inhibitor (at 6 and 24 h), as well as 400 × 400 nm test samples RGO, PRGO, and GO (6 h) showed significantly higher Cdc42 activation than the no GFN control condition. These results are consistent with extensive protrusions observed and measured from the exposure experiments with micropatterned cell pairs, as well as with the established role of filopodia on chemotaxis. In sum, our results show that ROCK inhibitor and the oxidized test GFNs affects Cdc42 activation much more than they influence Rac1. It is possible that these effects are not significantly demonstrated after 24 h due to the decrease in cellular viability at 50 µg/mL for some test GFNs (Fig. S1b). We also note that even though the reference graphene-treated cell pairs demonstrated protrusion formation (Fig. 4), no significant increase in Cdc42 or Rac1 was measured under this condition. This result indicates that GFN characteristics could influence the preference for the mechanism for protrusion formation. Due to the similarity in trends observed in cell pairs treated with ROCK inhibitor and test GFNs, we can infer from the results of G-LISA activation assays and quantification of HUVEC cell pair morphology that GFN-triggered cytoplasmic protrusions are not solely nor predominantly controlled by small GTPase activation, but are also potentially driven by the ROCK inhibitory behavior of GFNs.

2.4. Perturbation of ROCK activity due to GFNs

To test the hypothesis that GFNs can act as ROCK inhibitors, a dose-dependent (5–75 μ g/mL) ROCK activity assay was performed after 30 min of incubation of GFNs with assay reagents (see Supporting Information for more details on the method). ROCK is involved in many processes that regulate actin organization and contractility (Kümper et al., 2016; Yao et al., 2010). During inflammation, it is well established that ROCK activity becomes stimulated to trigger F-actin to elongate radially and form stress fibers, followed by vascular hyperpermeability (Beckers et al., 2015; Breslin et al., 2015). The ROCK inhibitory behavior of GFNs may seem counterintuitive then, since the permeability measurements for RGO-, PRGO-, and GO-treated HUVEC monolayers were higher than the no GFN condition, but the composite images of GFN-treated pairs do not show significant stress fiber formation similar to the Rho activator (calpeptin)-treated control (Fig. 1d). However, it is important to note that there are 2 isoforms of ROCK involved in the regulation of vascular endothelial hyperpermeability response: ROCK1 that is known to activate stress

fiber formation, and ROCK2 that is dispensable for stress fiber formation but still has been shown to regulate thrombin receptor-mediated vascular permeability (Beckers et al., 2015). To note, the ROCK inhibitor control used throughout this work, Y-27632, inhibits both Rho kinase isoforms. For the assay we used, we specifically tested the direct effect of GFNs on the activity of ROCK2. The ROCK2 activity was measured based on ROCK2-induced phosphorylation of a recombinant MYPT1 (myosin phosphatase target subunit 1), measured through the absorbance of the tetramethylbenzidine substrate at 450 nm. Results show a dose-dependent increase in inhibition of ROCK2 activity due to GFNs (Fig. 5c). Furthermore, the more oxidized GFNs demonstrated more ROCK2 inhibitory behavior. All three more oxidized, 400 nm GFNs potentiate ROCK2 inhibition much more significantly than the native graphene.

Attributing the extensive protrusion formation of cell pairs to ROCK2 inhibitory behavior is consistent with a previous report involving leukocytes, whereby inhibition of ROCK2 induces remodeling of actin cytoskeleton towards extensive formation of membrane protrusions due to increased integrin adhesion and phosphotyrosine signaling (Worthylake and Burridge, 2003). Endothelial cells patterned on gelatin fibrils have also been reported to exhibit abnormally long protrusions under culture conditions due to ROCK2 inhibition (Xue et al., 2014). Additionally, the apparent inhibition of Rho/ROCK pathway may be influenced by the interactions of GFNs with growth factors and cell adhesion molecules that participate in G-protein signaling involved in regulating RhoA (Marjoram et al., 2014). It is also worth noting that small molecules adsorb on the surface of GFNs to form biomolecular coronas that depend on the surface chemistry of the particle (Mei et al., 2018), small molecules essential for cell growth (e.g., amino acids, vitamins) have been shown to physisorb on carbon-based ENMs (Guo et al., 2008), and GO readily complexes with nucleic acids (de Lázaro et al., 2019). Such interactions may alter their bio-accessibility and could partly explain changes in the activity of the Rho/ROCK pathway. Importantly, while it is possible that there are other downstream effectors of the Rho/ROCK signaling pathway that interact or are influenced by the presence of GFNs, our results uncover how GFNs could influence a signaling pathway that regulates the formation of membrane protrusions relevant to barrier function and angiogenic migration (Fig. 5d).

3. Conclusion

In this study, we investigated the hierarchical surface oxidation-dependent effects of graphene family nanomaterials (GFNs) on vascular endothelial cells. Specifically, we tested the hypothesis that the surface chemistry of GFNs differentially affects the Rho/ROCK-mediated cytoskeletal organization of endothelial cells and endothelial barrier function. Formation of extensive cytoplasmic protrusions was quantified at different timepoints after exposure of micropatterned endothelial cell pairs to GFNs with varying surface oxidation. Our results suggest that higher surface oxidation of GFN corresponds to higher endothelial permeability and that all test GFNs at 50 μ g/mL resulted in the formation of endothelial cytoplasmic protrusions. By measuring the changes in Rac and Cdc42 GTPase activation after GFN exposure, we found that the more oxidized GFNs (RGO, PRGO, GO) induced an increased activity of the filopodia-promoting Cdc42 activity but not the lamellipodia-promoting Rac GTPase. These results, together with the measured decrease in ROCK

activity in the presence of the more oxidized test GFNs, suggest that the GFN-triggered cytoplasmic protrusions can be influenced by the oxidation-dependent ROCK inhibitory behavior of GFNs. In the future, it would be of interest to decouple the effects of size and GFN oxidation, as well as elucidating whether the effects reported in this work can be primarily attributed to the influence of GFN internalization or the mechanical stress GFNs may cause upon their edge-interaction with cell membranes as 2DNMs. Another important subject of future studies would be to elucidate why these GFNs preferentially inhibits ROCK and activates Cdc42 over Rac1. Collectively, our results provided insights on how surface chemistry of materials could be potentially utilized to systematically influence biochemical signaling pathways in cells, enabling more controlled cell-material interactions.

Supplementary Material

Refer to Web version on PubMed Central for supplementary material.

Acknowledgements

This study was supported by the National Institute of Environmental Health Sciences of the National Institutes of Health (Award Number U01ES027272) as part of the Nanotechnology Health Implications Research (NHIR) Consortium. The content is solely the responsibility of the authors and does not necessarily represent the official views of the National Institutes of Health. The synthesis and characterization of engineered nanomaterials in the research presented in this publication was performed by the Engineered Nanomaterials Resource and Coordination Core (ERCC) at the Center for Nanotechnology and Nanotoxicology at the T.H. Chan Harvard School of Public Health, part of the NIEHS/NHIR consortium under Award Number (Award Number U24ES026946). This work was partially supported by the Wyss Institute for Biologically Inspired Engineering at Harvard University and by the National Science Foundation through the Harvard University Materials Research Science and Engineering Center (MRSEC) DMR-2011754. For soft lithography work, we thank the Harvard Center for Nanoscale Systems (CNS), a member of the National Nanotechnology Infrastructure Network (NNIN) under NSF Award No. 1541959. H. A. M. A. would like to thank the American Chemical Society for generous support through the Irving S. Sigal Postdoctoral Fellowship. We acknowledge Mr. Daniel Drennan for providing technical assistance and Mr. Michael Rosnach for the graphical illustrations.

Abbreviations:

2DNMs 2-D nanomaterials

8-CPT-cAMP 8-(4-chlorophenylthio)adenosine 3',5'-cyclic

monophosphate

FLG few-layer graphene

GFNs graphene family nanomaterials

GO graphene oxide

HUVEC human umbilical vein endothelial cell

MTS 3-(4,5-dimethylthiazol-2-yl)-5-(3-

carboxymethoxyphenyl)-2-(4-sulfophenyl)-2H-tetrazolium

MYPT1 myosin phosphatase target subunit 1

PRGO partially reduced graphene oxide

RGO reduced graphene oxide

ROCK Rho-associated kinase

ROS reactive oxygen species

References

Alnasser F, Castagnola V, Boselli L, Esquivel-Gaon M, Efeoglu E, McIntyre J, Byrne HJ, Dawson KA, 2019. Graphene nanoflake uptake mediated by scavenger receptors. Nano Lett. 19, 1260–1268. [PubMed: 30628448]

- Bazina L, Bitounis D, Cao X, DeLoid G, Parviz D, Strano M, Lin H-Y, Bell DC, Thrall BD, Demokritou P, 2021. Biotransformations and cytotoxicity of eleven graphene and inorganic twodimensional nanomaterials using simulated digestions coupled with a triculture in vitro model of the human gastrointestinal epithelium. Environ. Sci. Nano 8, 3233–3249.
- Beckers CML, Knezevic N, Valent ET, Tauseef M, Krishnan R, Rajendran K, Hardin CC, Aman J, van Bezu J, Sweetnam P, et al., 2015. ROCK2 primes the endothelium for vascular hyperpermeability responses by raising baseline junctional tension. Vasc. Pharmacol 70, 45–54.
- Belvitch P, Htwe YM, Brown ME, Dudek S, 2018. Cortical actin dynamics in endothelial permeability. Curr. Top. Membr 82, 141–195. [PubMed: 30360779]
- Bengtson S, Knudsen KB, Kyjovska ZO, Berthing T, Skaug V, Levin M, Koponen IK, Shivayogimath A, Booth TJ, Alonso B, et al., 2017. Differences in inflammation and acute phase response but similar genotoxicity in mice following pulmonary exposure to graphene oxide and reduced graphene oxide. PLoS One 12, e0178355. [PubMed: 28570647]
- Bhattacharya K, Mukherjee SP, Gallud A, Burkert SC, Bistarelli S, Bellucci S, Bottini M, Star A, Fadeel B, 2016. Biological interactions of carbon-based nanomaterials: from coronation to degradation. Nanomedicine 12, 333–351. [PubMed: 26707820]
- Bisaria A, Hayer A, Garbett D, Cohen D, Meyer T, 2020. Membrane-proximal F-actin restricts local membrane protrusions and directs cell migration. Science 368, 1205–1210. [PubMed: 32527825]
- Bischoff I, Hornburger MC, Mayer BA, Beyerle A, Wegener J, Fürst R, 2016. Pitfalls in assessing microvascular endothelial barrier function: impedance-based devices versus the classic macromolecular tracer assay. Sci. Rep 6, 23671. [PubMed: 27025965]
- Bitounis D, Pyrgiotakis G, Bousfield D, Demokritou P, 2019. Dispersion preparation, characterization, and dosimetric analysis of cellulose nano-fibrils and nano-crystals: implications for cellular toxicological studies. NanoImpact 15. 10.1016/j.impact.2019.100171.
- Bitounis D, Parviz D, Cao X, Amadei CA, Vecitis CD, Sunderland EM, Thrall BD, Fang M, Strano MS, Demokritou P, 2020. Synthesis and physicochemical transformations of size-sorted graphene oxide during simulated digestion and its toxicological assessment against an in vitro model of the human intestinal epithelium. Small 16, e1907640. [PubMed: 32196921]
- Bogatcheva NV, Verin AD, 2008. The role of cytoskeleton in the regulation of vascular endothelial barrier function. Microvasc. Res 76, 202–207. [PubMed: 18657550]
- Breslin JW, Zhang XE, Worthylake RA, Souza-Smith FM, 2015. Involvement of local lamellipodia in endothelial barrier function. PLoS One 10, e0117970. [PubMed: 25658915]
- Chng ELK, Pumera M, 2015. Toxicity of graphene related materials and transition metal dichalcogenides. RSC Adv. 5, 3074–3080.
- Claesson-Welsh L, Dejana E, McDonald DM, 2021. Permeability of the endothelial barrier: identifying and reconciling controversies. Trends Mol. Med 27, 314–331. [PubMed: 33309601]
- Contreras-Torres FF, Rodríguez-Galván A, Guerrero-Beltrán CE, Martínez-Lorán E, Vázquez-Garza E, Ornelas-Soto N, García-Rivas G, 2017. Differential cytotoxicity and internalization of graphene family nanomaterials in myocardial cells. Mater. Sci. Eng C 73, 633–642.
- de Lázaro I, Vranic S, Marson D, Rodrigues AF, Buggio M, Esteban-Arranz A, Mazza M, Posocco P, Kostarelos K, 2019. Graphene oxide as a 2D platform for complexation and intracellular delivery of siRNA. Nanoscale 11, 13863–13877. [PubMed: 31298676]

DeLoid GM, Cohen JM, Pyrgiotakis G, Demokritou P, 2017. Preparation, characterization, and in vitro dosimetry of dispersed, engineered nanomaterials. Nat. Protoc 12, 355–371. [PubMed: 28102836]

- Duan Y, Coreas R, Liu Y, Bitounis D, Zhang Z, Parviz D, Strano M, Demokritou P, Zhong W, 2020. Prediction of protein corona on nanomaterials by machine learning using novel descriptors. NanoImpact 17.
- Dudek SM, Garcia JG, 2001. Cytoskeletal regulation of pulmonary vascular permeability. J. Appl. Physiol 1985 (91), 1487–1500.
- Eweje F, Ardona HAM, Zimmerman JF, O'Connor BB, Ahn S, Grevesse T, Rivera KN, Bitounis D, Demokritou P, Parker KK, 2019. Quantifying the effects of engineered nanomaterials on endothelial cell architecture and vascular barrier integrity using a cell pair model. Nanoscale 11, 17878–17893. [PubMed: 31553035]
- Fadeel B, Bussy C, Merino S, Vazquez E, Flahaut E, Mouchet F, Evariste L, Gauthier L, Koivisto AJ, Vogel U, et al., 2018. Safety assessment of graphene-based materials: focus on human health and the environment. ACS Nano 12, 10582–10620. [PubMed: 30387986]
- Figueiredo AM, Barbacena P, Russo A, Vaccaro S, Ramalho D, Pena A, Lima AP, Ferreira RR, Fidalgo MA, El-Marjou F, et al., 2021. Endothelial cell invasion is controlled by dactylopodia. Proc. Natl. Acad. Sci 118, e2023829118. [PubMed: 33903241]
- Frontiñán-Rubio J, Gómez MV, Martín C, González-Domínguez JM, Durán-Prado M, Vázquez E, 2018. Differential effects of graphene materials on the metabolism and function of human skin cells. Nanoscale 10, 11604–11615. [PubMed: 29892760]
- Guo L, Von Dem Bussche A, Buechner M, Yan A, Kane AB, Hurt RH, 2008. Adsorption of essential micronutrients by carbon nanotubes and the implications for nanotoxicity testing. Small 4, 721–727. [PubMed: 18504717]
- Hobbs GA, Zhou B, Cox AD, Campbell SL, 2014. Rho GTPases, oxidation, and cell redox control. Small GTPases 5, e28579. [PubMed: 24809833]
- Holt BD, Arnold AM, Sydlik SA, 2021. The blanket effect: how turning the world upside down reveals the nature of graphene oxide cytocompatibility. Adv. Healthc. Mater 10, 2001761.
- Huang J, Zong C, Shen H, Liu M, Chen B, Ren B, Zhang Z, 2012. Mechanism of cellular uptake of graphene oxide studied by surface-enhanced Raman spectroscopy. Small 8, 2577–2584. [PubMed: 22641430]
- Kucki M, Diener L, Bohmer N, Hirsch C, Krug HF, Palermo V, Wick P, 2017. Uptake of label-free graphene oxide by Caco-2 cells is dependent on the cell differentiation status. J. Nanobiotechnology 15, 46. [PubMed: 28637475]
- Kümper S, Mardakheh FK, McCarthy A, Yeo M, Stamp GW, Paul A, Worboys J, Sadok A, Jørgensen C, Guichard S, et al., 2016. Rho-associated kinase (ROCK) function is essential for cell cycle progression, senescence and tumorigenesis. eLife 5, e12203. [PubMed: 26765561]
- Lamalice L, Le Boeuf F, Huot J, 2007. Endothelial cell migration during angiogenesis. Circ. Res 100, 782–794. [PubMed: 17395884]
- Li Y, Yuan H, von dem Bussche A, Creighton M, Hurt RH, Kane AB, Gao H, 2013. Graphene microsheets enter cells through spontaneous membrane penetration at edge asperities and corner sites. Proc. Natl. Acad. Sci. U. S. A 110, 12295–12300. [PubMed: 23840061]
- Li R, Guiney LM, Chang CH, Mansukhani ND, Ji Z, Wang X, Liao YP, Jiang W, Sun B, Hersam MC, et al., 2018. Surface oxidation of graphene oxide determines membrane damage, lipid peroxidation, and cytotoxicity in macrophages in a pulmonary toxicity model. ACS Nano 12, 1390–1402. [PubMed: 29328670]
- Li J, Wang X, Mei K-C, Chang CH, Jiang J, Liu X, Liu Q, Guiney LM, Hersam MC, Liao Y-P, et al., 2021. Lateral size of graphene oxide determines differential cellular uptake and cell death pathways in Kupffer cells, LSECs, and hepatocytes. Nano Today 37, 101061. [PubMed: 34055032]
- Liao KH, Lin YS, Macosko CW, Haynes CL, 2011. Cytotoxicity of graphene oxide and graphene in human erythrocytes and skin fibroblasts. ACS Appl. Mater. Interfaces 3, 2607–2615. [PubMed: 21650218]
- Marjoram RJ, Lessey EC, Burridge K, 2014. Regulation of RhoA activity by adhesion molecules and mechanotransduction. Curr. Mol. Med 14, 199–208. [PubMed: 24467208]

Matesanz MC, Vila M, Feito MJ, Linares J, Goncalves G, Vallet-Regi M, Marques PA, Portoles MT, 2013. The effects of graphene oxide nanosheets localized on F-actin filaments on cell-cycle alterations. Biomaterials 34, 1562–1569. [PubMed: 23177613]

- Mei K-C, Ghazaryan A, Teoh EZ, Summers HD, Li Y, Ballesteros B, Piasecka J, Walters A, Hider RC, Mailänder V, et al., 2018. Protein-corona-by-design in 2D: a reliable platform to decode bio–nano interactions for the next-generation quality-by-design nanomedicines. Adv. Mater 30, 1802732.
- Murphy CJ, Vartanian AM, Geiger FM, Hamers RJ, Pedersen J, Cui Q, Haynes CL, Carlson EE, Hernandez R, Klaper RD, et al., 2015. Biological responses to engineered nanomaterials: needs for the next decade. ACS Cent. Sci 1, 117–123. [PubMed: 27162961]
- O'Connor BB, Grevesse T, Zimmerman JF, Ardoña HAM, Jimenez JA, Bitounis D, Demokritou P, Parker KK, 2020. Human brain microvascular endothelial cell pairs model tissue-level blood–brain barrier function. Integr. Biol 12, 64–79.
- Ou L, Song B, Liang H, Liu J, Feng X, Deng B, Sun T, Shao L, 2016. Toxicity of graphene-family nanoparticles: a general review of the origins and mechanisms. Part. Fibre Toxicol 13, 57. [PubMed: 27799056]
- Parker KK, Brock AL, Brangwynne C, Mannix RJ, Wang N, Ostuni E, Geisse NA, Adams JC, Whitesides GM, Ingber DE, 2002. Directional control of lamellipodia extension by constraining cell shape and orienting cell tractional forces. FASEB J. 16, 1195–1204. [PubMed: 12153987]
- Parviz D, Strano M, 2018. Endotoxin-free preparation of graphene oxide and graphene-based materials for biological applications. Curr. Protoc. Chem. Biol 10, e51. [PubMed: 30285316]
- Parviz D, Bitounis D, Demokritou P, Strano M, 2020. Engineering two-dimensional nanomaterials to enable structure-activity relationship studies in nanosafety research. NanoImpact 18.
- Pelin M, Fusco L, León V, Martín C, Criado A, Sosa S, Vázquez E, Tubaro A, Prato M, 2017. Differential cytotoxic effects of graphene and graphene oxide on skin keratinocytes. Sci. Rep 7, 40572. [PubMed: 28079192]
- Reina G, Gonzalez-Dominguez JM, Criado A, Vazquez E, Bianco A, Prato M, 2017. Promises, facts and challenges for graphene in biomedical applications. Chem. Soc. Rev 46, 4400–4416. [PubMed: 28722038]
- Rottner K, Schaks M, 2019. Assembling actin filaments for protrusion. Curr. Opin. Cell Biol 56, 53–63. [PubMed: 30278304]
- Sanchez VC, Jachak A, Hurt RH, Kane AB, 2012. Biological interactions of graphene-family nanomaterials: an interdisciplinary review. Chem. Res. Toxicol 25, 15–34. [PubMed: 21954945]
- Seabra AB, Paula AJ, de Lima R, Alves OL, Duran N, 2014. Nanotoxicity of graphene and graphene oxide. Chem. Res. Toxicol 27, 159–168. [PubMed: 24422439]
- Spindler V, Schlegel N, Waschke J, 2010. Role of GTPases in control of microvascular permeability. Cardiovasc. Res 87, 243–253. [PubMed: 20299335]
- Sydlik SA, Jhunjhunwala S, Webber MJ, Anderson DG, Langer R, 2015. In vivo compatibility of graphene oxide with differing oxidation states. ACS Nano 9, 3866–3874. [PubMed: 25849074]
- Thomas DG, Smith JN, Thrall BD, Baer DR, Jolley H, Munusamy P, Kodali V, Demokritou P, Cohen J, Teeguarden JG, 2018. ISD3: a particokinetic model for predicting the combined effects of particle sedimentation, diffusion and dissolution on cellular dosimetry for in vitro systems. Part. Fibre Toxicol 15, 6. [PubMed: 29368623]
- Toprani SM, Bitounis D, Huang Q, Oliveira N, Ng KW, Tay CY, Nagel ZD, Demokritou P, 2021. High-throughput screening platform for nanoparticle-mediated alterations of DNA repair capacity. ACS Nano 15, 4728–4746. [PubMed: 33710878]
- Tsygankov D, Bilancia CG, Vitriol EA, Hahn KM, Peifer M, Elston TC, 2014. CellGeo: a computational platform for the analysis of shape changes in cells with complex geometries. J. Cell Biol 204, 443–460. [PubMed: 24493591]
- Watson C, Ge J, Cohen J, Pyrgiotakis G, Engelward BP, Demokritou P, 2014. High-throughput screening platform for engineered nanoparticle-mediated genotoxicity using CometChip technology. ACS Nano 8, 2118–2133. [PubMed: 24617523]
- Worthylake RA, Burridge K, 2003. RhoA and ROCK promote migration by limiting membrane protrusions. J. Biol. Chem 278, 13578–13584. [PubMed: 12574166]

Wu C, Wang C, Han T, Zhou X, Guo S, Zhang J, 2013. Insight into the cellular internalization and cytotoxicity of graphene quantum dots. Adv Healthc Mater 2, 1613–1619. [PubMed: 23703800]

- Wu L, Zeng L, Jiang X, 2015. Revealing the nature of interaction between graphene oxide and lipid membrane by surface-enhanced infrared absorption spectroscopy. J. Am. Chem. Soc 137, 10052– 10055. [PubMed: 26222327]
- Xue N, Bertulli C, Sadok A, Huang YYS, 2014. Dynamics of filopodium-like protrusion and endothelial cellular motility on one-dimensional extracellular matrix fibrils. Interface Focus 4, 20130060. [PubMed: 24748955]
- Yao L, Romero MJ, Toque HA, Yang G, Caldwell RB, Caldwell RW, 2010. The role of RhoA/Rho kinase pathway in endothelial dysfunction. J. Cardiovasc. Dis. Res 1, 165–170. [PubMed: 21264179]
- Zimmerman JF, Parameswaran R, Murray G, Wang Y, Burke M, Tian B, 2016. Cellular uptake and dynamics of unlabeled freestanding silicon nanowires. Sci. Adv 2, e1601039. [PubMed: 28028534]
- Zou X, Wei S, Jasensky J, Xiao M, Wang Q, Brooks Iii CL, Chen Z, 2017. Molecular interactions between graphene and biological molecules. J. Am. Chem. Soc 139, 1928–1936. [PubMed: 28092440]

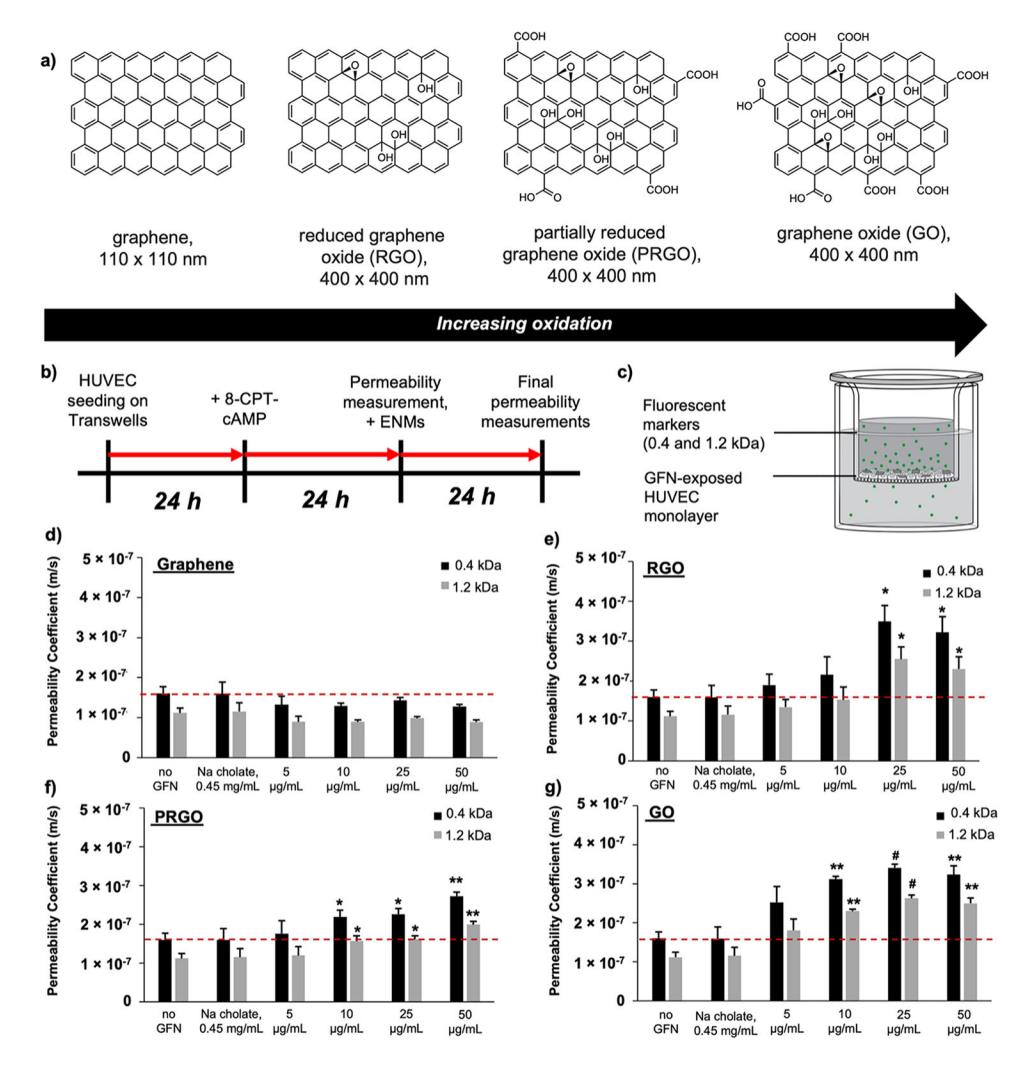


Fig. 1. (a) Molecular representation of GFNs investigated here. (b) Experimental timeline and (c) schematic illustration of the setup for permeability measurements. (d-g) Calculated permeability coefficients for HUVEC monolayers exposed to 50 μ g/mL GFNs for 24 h. n = 6; Error bars = s.e.m.; *p ≤ 0.05, **p ≤ 0.005, #p ≤ 0.001.

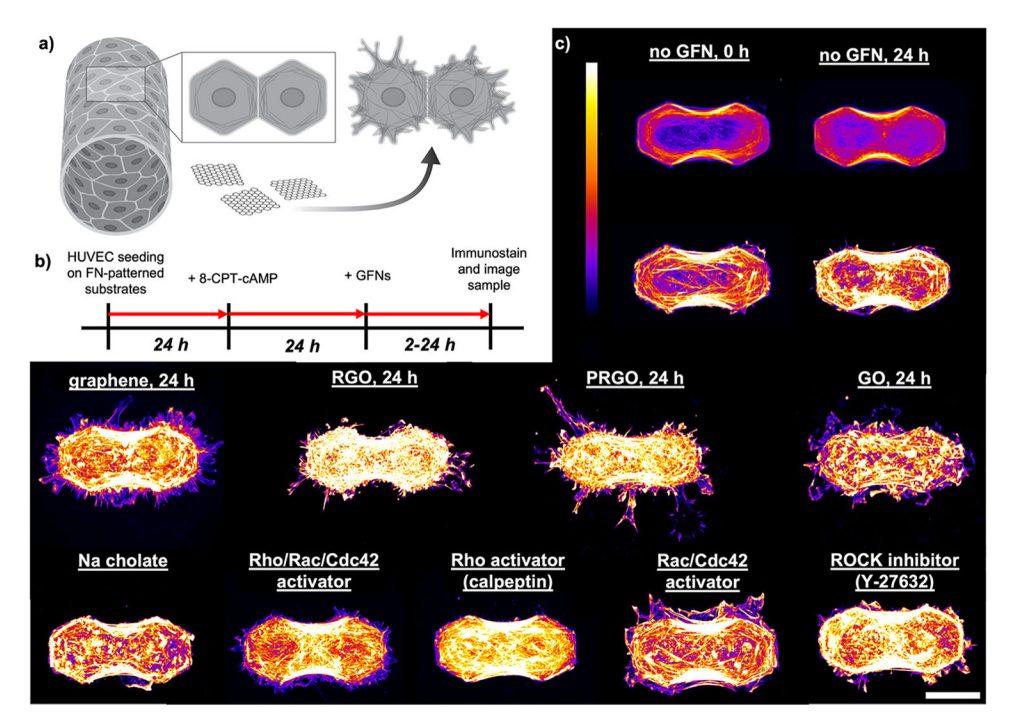


Fig. 2. (a) Schematic illustration of cell pairs as a reductionist model of an endothelial barrier. (b) Experimental timeline for cellular morphology and protrusion quantification using micropatterned cell pairs. (c) F-actin composite images of micropatterned cell pairs under different conditions. Top images for *no GFN* condition are F-actin composite images from average intensity projection. The rest of the images show the maximum intensity projection of multiple cell pairs under similar condition. n = 30-70 across at least three independent biological replicates; scale bar = 50 μ m.

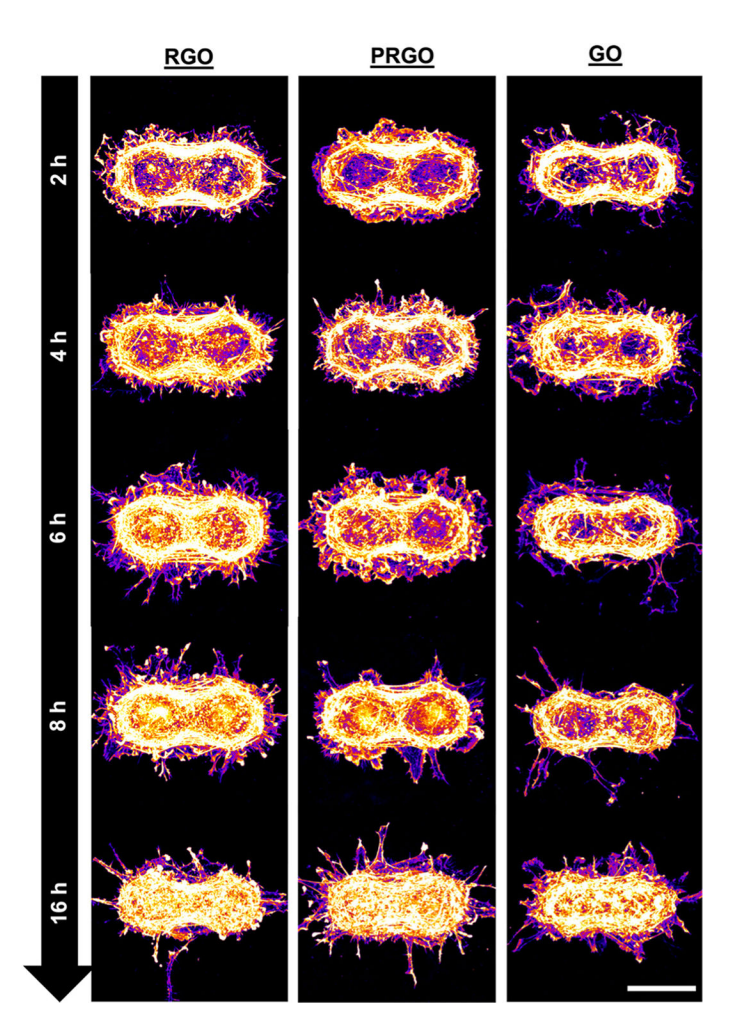


Fig. 3. Maximum intensity projection of F-actin of cell pairs exposed to RGO, PRGO, GO at multiple time points (2–16 h exposure of cell pairs to 50 μ g/mL GFNs). n = 30-70; scale bar = 50 μ m.

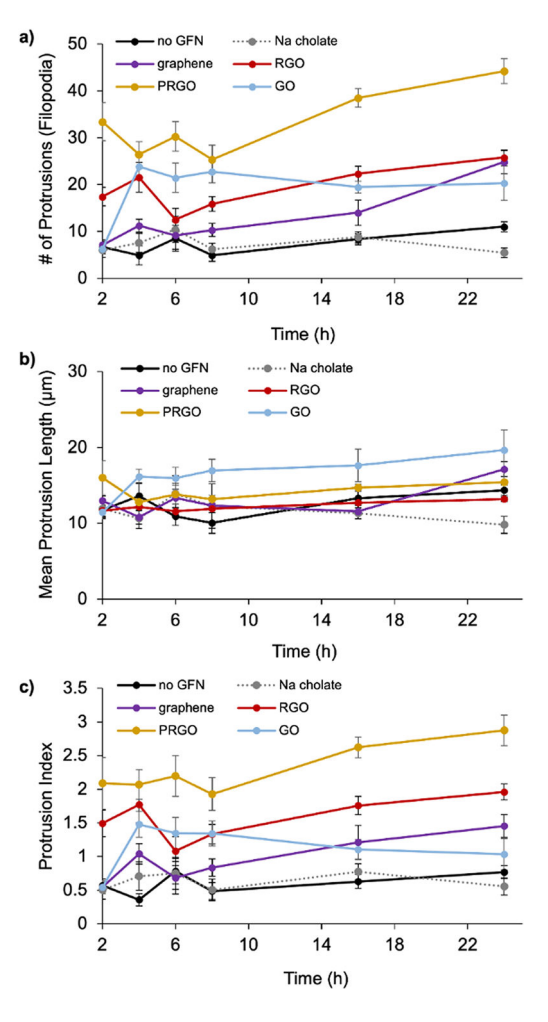


Fig. 4. Cell protrusion characterization at multiple time points under different exposure conditions: no ENM, 0.45 mg/mL Na cholate, and 50 μ g/mL GFNs. Using the distinction for filopodia as protrusions that are \geq 7 μ m length and \leq 7 μ m width, (a) number of protrusions per cell pair and (b) mean protrusion length per cell pair under each condition and timepoint were measured. (c) Protrusion index is reported as the number of protrusions/mean protrusion length. n = 30–70 across at least three independent biological replicates.

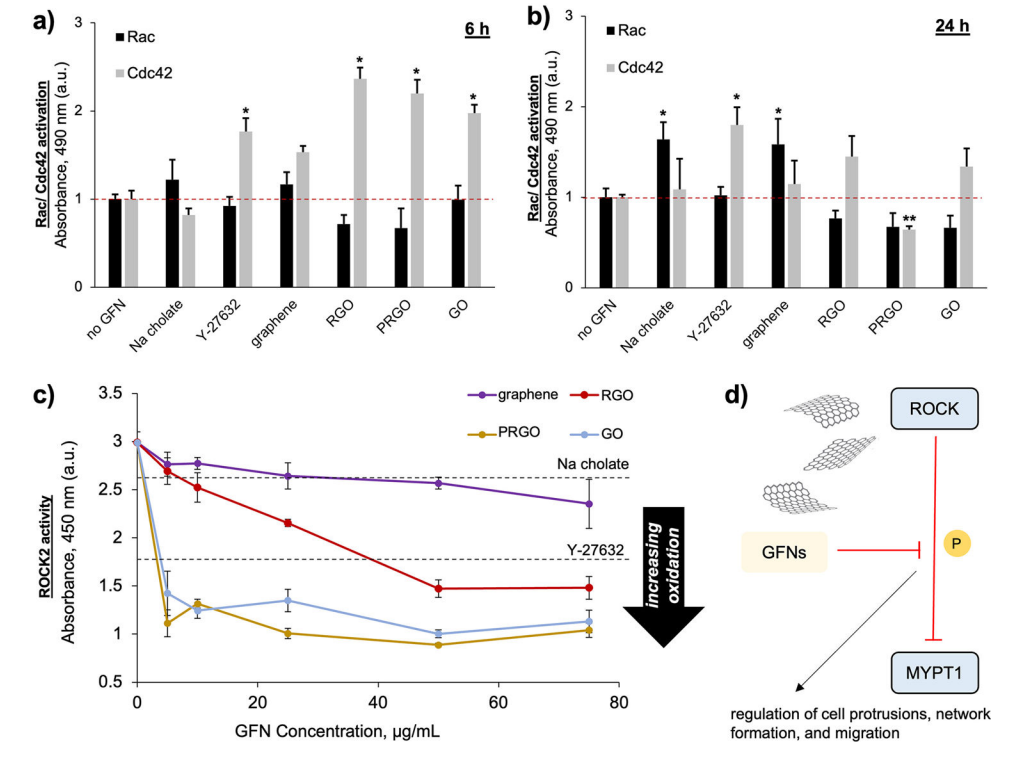


Fig. 5. (a) Rac and (b) Cdc42 activation assays (G-LISA) were used to assess the influence of GFN exposure to small GTPases in HUVECs. Serum-starved confluent layers of HUVECs were exposed to 50 µg/mL of GFNs, 10 µM Y-27632, and 0.45 mg/mL Na cholate. Measurements were taken at 6 and 24 h. n=4; Error bars = s.e. m.; * $p \le 0.05$, ** $p \le 0.005$. (c) ROCK activity at different concentrations of the GFNs under study (0–75 µg/mL); no GFN, Abs₄₅₀ = 2.99 ± 0.11; 0.45 mg/mL Na cholate, Abs₄₅₀ = 2.58 ± 0.21; 10 µM Y-27632, Abs₄₅₀ = 1.75 ± 0.11. n=3; Error bars = s.e.m. (d) Schematic illustrating the proposed ROCK inhibition of GFNs, which consequentially results in extensive cell protrusions, actin network destabilization, and increased tissue permeability observed here.